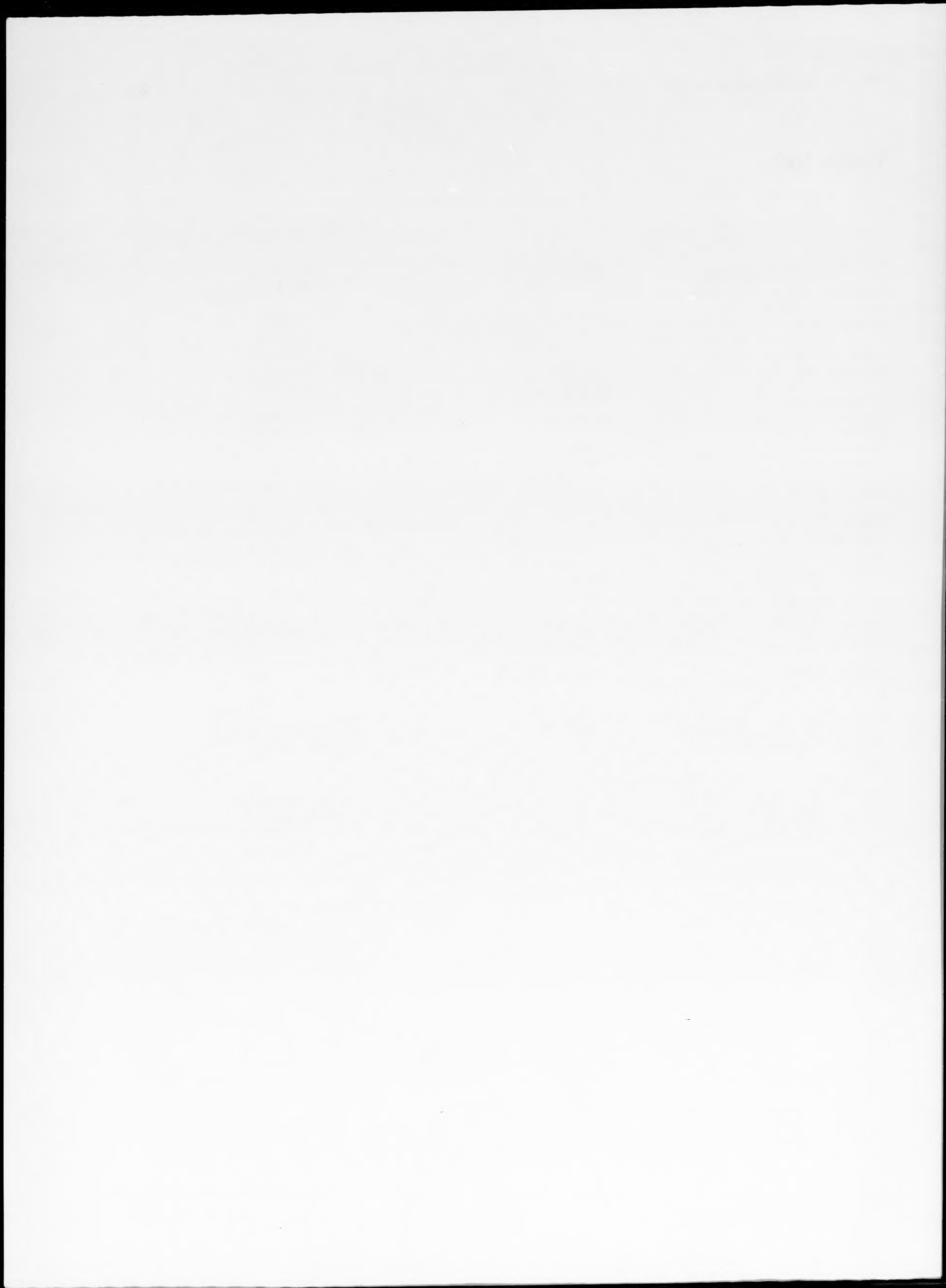


Author Index

- Atamert, S., 101
Banerjee, D., 151
Beaven, P. A., 173
Bhadeshia, H. K. D. H., 101
Čadek, J., 61, 165
Cousin, P., 119
Durman, M., 247
Edelson, L. H., 193
Es-Souni, M., 173
Evans, G. M., 173
Fiala, J., 61, 165
Geng, L., 113
Gialanella, S., 257
Grummon, D. S., 127
Guilemany, J. M., 241
Hoshiya, T., 185
Hsueh, C.-H., L11
Hu, X., 139
Ichihashi, Y., 185
Inal, O. T., 83, 205
Killen, P. D., 231
Kim, J. J., L7
Kieselev, I. K., 29
Kloc, L., 61, 165
Krupin, Yu. A., 29
Lal, D. N., 37
Lee, S., 1
Lee Pak, J. S., 83
Liu, Q., 113
Llorca-Isern, N., 241
Mannan, S. L., 67
Marchetti, F., 257
Margolin, H., 139
Meyers, C. A., 127
Milne, S. J., 263
Mishra, R. S., 151
Molinari, A., 257
Mostaghaci, H., 263
Mukherjee, K., 83
Murphy, S., 247
Nma, S. W., L7
Namboodhiri, T. K. G., 37
Ozbaysal, K., 205
Page, N. W., 231
Pak, H.-R., 185
Pak, H. R., 83
Pak, J. S. L., 83
Rabin, B. H., L1
Rao, K. B. S., 67
Ritchie, R. O., 193
Ross, R. A., 119
Ryu, J. H., L7
Sawalha, K., 247
Scardi, P., 257
Senior, B. A., 51
Smith, E., 11
St. John, D. H., 231
Takada, F., 185
Tewari, S. N., 219
Tiziani, A., 257
Turčič, B., 17, 21
Valsan, M., 67
Wang, S.-D., 1
Wang, W., 93
Wu, K., 113
Xu, Y., 93
Yao, C. K., 113



Subject Index

- Alloying**
relationships between microstructure and properties of unalloyed compacted graphite cast irons, 241
- Alloys**
creep in a Cu-14at.%Al solid solution alloy at intermediate temperatures and low stresses, 165
crystal structures and microstructures of (Ni,Cu)₃Sn alloys, 83
electron metallographic study of the commercial zinc-based pressure-die-cast alloy 3, 247
microstructure and stability of Fe-Cr-C hardfacing alloys, 101
restoration phenomena of neutron-irradiated Ti-Ni shape memory alloys, 185
- Aluminium**
creep in a Cu-14at.%Al solid solution alloy at intermediate temperatures and low stresses, 165
microdiffraction study of β -SiC whiskers in an SiC_w-6061Al composite, 113
microstructural characterization of α_2 +B2 titanium aluminide intermetallic (super- α_2) using transmission electron microscopy, 193
microstructure and steady state creep in Ti-24Al-11Nb, 151
- Carbon**
joining of fiber-reinforced SiC composites by *in situ* reaction methods, L1
microdiffraction study of β -SiC whiskers in an SiC_w-6061Al composite, 113
microstructure and stability of Fe-Cr-C hardfacing alloys, 101
microstructure of copper-bearing C-Mn weld metal: as-welded and stress-relieved states, 173
thermodynamics and structure of solidification in the fusion zone of CO₂ laser welds of 15-5 PH stainless steel, 205
- Cavitation**
cavitation damage in AISI type 347 weld metal arising from creep deformation, 51
- Chromium**
microstructure and stability of Fe-Cr-C hardfacing alloys, 101
- Cobalt**
study of the diamond-matrix interface in hot-pressed cobalt-based tools, 257
- Compaction**
relationships between microstructure and properties of unalloyed compacted graphite cast irons, 241
sintering enhancement in dynamically compacted commercial iron powders, 231
- Composites**
fatigue damage periods in composite laminates, 17
joining of fiber-reinforced SiC composites by *in situ* reaction methods, L1
microdiffraction study of β -SiC whiskers in an SiC_w-6061Al composite, 113
"natural" phenomenological fatigue damage cumulation model for composite laminates, 21
- Copper**
creep in a Cu-14at.%Al solid solution alloy at intermediate temperatures and low stresses, 165
crystal structures and microstructures of (Ni,Cu)₃Sn alloys, 83
microstructure of copper-bearing C-Mn weld metal: as-welded and stress-relieved states, 173
- Corrosion**
effect of structural factors on corrosion crack resistance parameters, 29
- Crack extension**
crack extension in a material whose resistance to deformation increases with increasing strain, 11
- Crack initiation**
sensitivity of surface crack initiation to surface roughness in low-cycle fatigue at high temperature, 507
- Crack propagation**
model for the effect of mean stress on the threshold condition for fatigue crack propagation, 37
- Crack resistance**
effect of structural factors on corrosion crack resistance parameters, 29
- Cracks**
analysis of the elastic interaction between an edge dislocation and an internal crack, 1
crack extension in a material whose resistance to deformation increases with increasing strain, 11
effect of structural factors on corrosion crack resistance parameters, 29
model for the effect of mean stress on the threshold condition for fatigue crack propagation, 37
- Creep**
cavitation damage in AISI type 347 weld metal arising from creep deformation, 51
creep in a Cu-14at.%Al solid solution alloy at intermediate temperatures and low stresses, 165
microstructure and steady state creep in Ti-24Al-11Nb, 151
new procedure to evaluate creep data obtained by the helioid spring specimen technique under conditions of non-viscous creep behaviour, 61
- Crystal nucleation**
crystal nucleation and glass formation in undercooled Pd-Ni-P melts, 93
- Crystal structures**
crystal structures and microstructures of (Ni,Cu)₃Sn alloys, 83
- Deformation**
cavitation damage in AISI type 347 weld metal arising from creep deformation, 51

- crack extension in a material whose resistance to deformation increases with increasing strain, 11
- Dendrite**
dendrite tip radii in directionally solidified Pb-8.4at.%Au, 219
- Diamond**
study of the diamond-matrix interface in hot-pressed cobalt-based tools, 257
- Dislocations**
analysis of the elastic interaction between an edge dislocation and an internal crack, 1
dislocation distributions in non-uniform stress fields, 139
- Drying**
influence of different drying conditions on powder properties and processing characteristics, 263
- Elasticity**
analysis of the elastic interaction between an edge dislocation and an internal crack, 1
- Electron metallography**
electron metallographic study of the commercial zinc-based pressure-die-cast alloy 3, 247
- Fatigue**
fatigue damage periods in composite laminates, 17
finite element model of persistent slip band interaction with strengthened surface films during low cycle fatigue, 127
model for the effect of mean stress on the threshold condition for fatigue crack propagation, 37
"natural" phenomenological fatigue damage cumulation model for composite laminates, 21
sensitivity of surface crack initiation to surface roughness in low-cycle fatigue at high temperature, L7
strain-controlled low cycle fatigue behaviour of type 304 stainless steel base material, type 308 stainless steel weld metal and 304-308 stainless steel weldments, 67
- Fibre pull-out**
theoretical comparison of two loading methods in fiber pull-out tests, L11
- Fibres**
joining of fiber-reinforced SiC composites by *in situ* reaction methods, L1
theoretical comparison of two loading methods in fiber pull-out tests, L11
- Finite element modelling**
finite element model of persistent slip band interaction with strengthened surface films during low cycle fatigue, 127
- Fusion zone**
thermodynamics and structure of solidification in the fusion zone of CO₂ laser welds of 15-5 PH stainless steel, 205
- Glass**
crystal nucleation and glass formation in undercooled Pd-Ni-P melts, 93
- Gold**
dendrite tip radii in directionally solidified Pb-8.4at.%Au, 219
- Graphite**
relationships between microstructure and properties of unalloyed compacted graphite cast irons, 241
- Helicoid spring specimen technique**
new procedure to evaluate creep data obtained by the helicoid spring specimen technique under conditions of non-viscous creep behaviour, 61
- Hot pressing**
study of the diamond-matrix interface in hot-pressed cobalt-based tools, 257
- Interfaces**
study of the diamond-matrix interface in hot-pressed cobalt-based tools, 257
- Iron**
microstructure and stability of Fe-Cr-C hardfacing alloys, 101
relationships between microstructure and properties of unalloyed compacted graphite cast irons, 241
sintering enhancement in dynamically compacted commercial iron powders, 231
- Joining**
joining of fiber-reinforced SiC composites by *in situ* reaction methods, L1
- Laminates**
fatigue damage periods in composite laminates, 17
"natural" phenomenological fatigue damage cumulation model for composite laminates, 21
- Lead**
dendrite tip radii in directionally solidified Pb-8.4at.%Au, 219
- Loading**
theoretical comparison of two loading methods in fiber pull-out tests, 511
- Manganese**
microstructure of copper-bearing C-Mn weld metal: as-welded and stress-relieved states, 173
- Mechanical properties**
relationships between microstructure and properties of unalloyed compacted graphite cast irons, 241
- Melts**
crystal nucleation and glass formation in undercooled Pd-Ni-P melts, 93
- Microdiffraction**
microdiffraction study of β -SiC whiskers in an SiC_w/6061Al composite, 113
- Microstructure**
crystal structures and microstructures of (Ni,Cu)₃Sn alloys, 83
microstructural characterization of α_2 + B2 titanium aluminide intermetallic (super- α_2) using transmission electron microscopy, 193
microstructure and stability of Fe-Cr-C hardfacing alloys, 101
microstructure and steady state creep in Ti-24Al-11Nb, 151
microstructure of copper-bearing C-Mn weld metal: as-welded and stress-relieved states, 173
relationships between microstructure and properties of unalloyed compacted graphite cast irons, 241

- Neutron irradiation
restoration phenomena of neutron-irradiated Ti-Ni shape memory alloys, 185
- Nickel
crystal nucleation and glass formation in undercooled Pd-Ni-P melts, 93
crystal structures and microstructures of (Ni,Cu)₃Sn alloys, 83
restoration phenomena of neutron-irradiated Ti-Ni shape memory alloys, 185
- Niobium
microstructure and steady state creep in Ti-24Al-11Nb, 151
- Oxides
preparation of mixed oxides: a review, 119
- Oxygen
thermodynamics and structure of solidification in the fusion zone of CO₂ laser welds of 15-5 PH stainless steel, 205
- Palladium
crystal nucleation and glass formation in undercooled Pd-Ni-P melts, 93
- Persistent slip bands
finite element model of persistent slip band interaction with strengthened surface films during low cycle fatigue, 127
- Phosphorus
crystal nucleation and glass formation in undercooled Pd-Ni-P melts, 93
- Powders
sintering enhancement in dynamically compacted commercial iron powders, 231
influence of different drying conditions on powder properties and processing characteristics, 263
- Pressure die casting
electron metallographic study of the commercial zinc-based pressure-die-cast alloy 3, 247
- Reinforcement
joining of fiber-reinforced SiC composites by *in situ* reaction methods, L1
- Shape memory alloys
restoration phenomena of neutron-irradiated Ti-Ni shape memory alloys, 185
- Silicon
joining of fiber-reinforced SiC composites by *in situ* reaction methods, L1
microdiffraction study of β -SiC whiskers in an SiC_w-6061Al composite, 113
- Sintering
sintering enhancement in dynamically compacted commercial iron powders, 231
- Solid solutions
creep in a Cu-14at.%Al solid solution alloy at intermediate temperatures and low stresses, 165
- Solidification
dendrite tip radii in directionally solidified Pb-8.4at.%Au, 219
thermodynamics and structure of solidification in the fusion zone of CO₂ laser welds of 15-5 PH stainless steel, 205
- Stability
microstructure and stability of Fe-Cr-C hardfacing alloys, 101
- Stainless steel
strain-controlled low cycle fatigue behaviour of type 304 stainless steel base material, type 308 stainless steel weld metal and 304-308 stainless steel weldments, 67
thermodynamics and structure of solidification in the fusion zone of CO₂ laser welds of 15-5 PH stainless steel, 205
- Strain
crack extension in a material whose resistance to deformation increases with increasing strain, 11
strain-controlled low cycle fatigue behaviour of type 304 stainless steel base material, type 308 stainless steel weld metal and 304-308 stainless steel weldments, 67
- Strengthening
finite element model of persistent slip band interaction with strengthened surface films during low cycle fatigue, 127
- Stress
model for the effect of mean stress on the threshold condition for fatigue crack propagation, 37
creep in a Cu-14at.%Al solid solution alloy at intermediate temperatures and low stresses, 165
dislocation distributions in non-uniform stress fields, 139
microstructure of copper-bearing C-Mn weld metal: as-welded and stress-relieved states, 173
- Structure
effect of structural factors on corrosion crack resistance parameters, 29
thermodynamics and structure of solidification in the fusion zone of CO₂ laser welds of 15-5 PH stainless steel, 205
- Surface roughness
sensitivity of surface crack initiation to surface roughness in low-cycle fatigue at high temperature, L7
- Thermodynamics
thermodynamics and structure of solidification in the fusion zone of CO₂ laser welds of 15-5 PH stainless steel, 205
- Tin
crystal structures and microstructures of (Ni,Cu)₃Sn alloys, 83
- Titanium
microstructural characterization of α_2 +B2 titanium aluminide intermetallic (super- α_2) using transmission electron microscopy, 193
microstructure and steady state creep in Ti-24Al-11Nb, 151
restoration phenomena of neutron-irradiated Ti-Ni shape memory alloys, 185
- Transmission electron microscopy
microstructural characterization of α_2 +B2 titanium aluminide intermetallic (super- α_2) using transmission electron microscopy, 193
- Weld metals
cavitation damage in AISI type 347 weld metal arising from creep deformation, 51
microstructure of copper-bearing C-Mn weld metal: as-welded and stress-relieved states, 173

strain-controlled low cycle fatigue behaviour of type 304 stainless steel base material, type 308 stainless steel weld metal and 304-308 stainless steel weldments, 67

Weldments

strain-controlled low cycle fatigue behaviour of type 304 stainless steel base material, type 308 stainless steel weld metal and 304-308 stainless steel weldments, 67

Welds

thermodynamics and structure of solidification in the

fusion zone of CO₂ laser welds of 15-5 PH stainless steel, 205

Whiskers

microdiffraction study of β -SiC whiskers in an SiC_w-6061Al composite, 113

Zinc

electron metallographic study of the commercial zinc-based pressure-die-cast alloy 3, 247

